Hindawi
Advances in Materials Science and Engineering
Volume 2019, Article ID 3420349, 14 pages
https://doi.org/10.1155/2019/3420349

Research Article

Mechanical Recovery of Cracked Fiber-Reinforced Mortar Incorporating Crystalline Admixture, Expansive Agent, and Geomaterial

Abdul Salam Buller,[1] **Fahad ul Rehman Abro**,[1] **Kwang-Myong Lee**,[1] **and Seung Yup Jang**[2]

[1]*Department of Civil, Architectural and Environmental System Engineering, Sungkyunkwan University (SKKU) 2066, Seobu-Ro, Jangan-Gu, Suwodn-Si, Gyeonggi-Do 16419, Republic of Korea*
[2]*Graduate School of Transportation, Korea National University of Transportation, Uiwang, Gyeonggi-do 16106, Republic of Korea*

Correspondence should be addressed to Kwang-Myong Lee; leekm79@skku.edu

Received 17 May 2019; Accepted 29 August 2019; Published 22 September 2019

Academic Editor: Ivan Giorgio

This research is sought to characterize the stimulated autogenous healing of fiber-reinforced mortars that incorporate healing agents such as crystalline admixtures, expansive agents, and geomaterials. The effects of the healing materials on mechanical performance and water permeability were evaluated experimentally. Furthermore, microscopic and microstructural observations were conducted to investigate the characteristics and physical appearance of healing products within healed cracks. Test results are presented herein regarding index of strength recovery (ISR), index of damage recovery (IDR) and index of dissipation energy gain (IDEG) in relation to crack healing, and reduction of water flow rate. The self-healing capability of the mortars was greater in terms of resisting water flow rather than recovering mechanical performance likely because water flow depends on surface crack sealing, whereas mechanical performance depends on bonding capacity as well as full-depth healing of cracks; thus, mechanical performance may further be improved after longer healing duration.

1. Introduction

Cracking is unavoidable during the service life of concrete structures. Cracking arises as a part of structural degradation from causes such as volumetric changes, hydration heating, and severe environmental stress. Cracks can serve as pathways for various hazardous agents, which can worsen the durability and lifespan of concrete structures [1]. Recently, various self-healing techniques have been developed and applied to extend the service life of concrete structures and reduce CO_2 emissions; such self-healing can overcome cracking and more generally enhance mechanical performance and durability [2, 3]. The maintenance cost of concrete structures, rigid pavements, and tunnels is equal to half of the annual construction budget in Europe [1]. Self-healing of cracked concrete can thus save a huge amount of money and time and no doubt would be highly beneficial for improving structures' long-term sustainability [4].

In various studies, the self-healing of concretes incorporating self-healing materials such as minerals, crystalline admixtures [5], bacteria [6, 7], PVA fibers [8–11], superabsorbent polymers (SAP) [12], and geomaterials [13] was investigated. Moreover, some investigations were also carried out to study the damage in generalized continuum framework which helps in linear modelling [14–16]. Ferrara et al. [17] suggested the fracture testing-based approach to assess the self-healing performance such as damage recovery and load recovery in concretes containing crystalline admixtures. Nishiwaki et al. [18] reported that crack width less than 100 μm strongly affects watertightness and recovery of energy absorption capacity. Choi et al. [19] examined the effective dispersion of crack in cementitious composites and

found that the restoration of watertightness through self-healing process was achieved due to the precipitation of $CaCO_3$. Herbert and Li [20] found that the stiffness and first cracking strength increase with increasing duration of healing at various strain levels. Van Tittelboom et al. [21] studied the effect of mix composition on the extent of autogenous self-healing and reported that crack healing can be improved by continued hydration or calcium hydration.

The mechanism of autogenous healing in concretes including various mineral admixtures was examined by Ahn and Kishi [22] through water permeability testing and microstructural study by means of SEM and XRD. Recently, Qureshi et al. [23] investigated the impacts of expansive mineral additives on the basis of flexural recovery and gas permeability. However, in works regarding the self-healing of concrete using expansive agents and crystalline materials, there have been few reports that specifically focus on the energy dissipation capacity of the concrete/mortar [24, 25].

An objective of the present study was to assess the effect of stimulated autogenous healing on the recovery of the mechanical performance of cracked fiber-reinforced mortars including healing agents such as crystalline admixtures (sodium carbonate and calcium stearate), expansive agents (calcium sulfoaluminate admixture), and geomaterials. The recovery of mechanical performance was studied in terms of index of strength recovery (ISR) and index of damage recovery (IDR). We also propose a new assessment technique based on the index of dissipation energy gain (IDEG). Water permeability testing was conducted, and the physical appearance of the healing products at the crack zones was observed by means of SEM and EDS analyses. Finally, the recovery rates of mechanical performance and watertightness were compared with respect to the initial crack widths and the self-healing agents used. Test results showed that, for large cracks, surface sealing of cracks with the use of healing agents is more effective in recovering watertightness than mechanical performance; that is, mechanical performance recovery was more complete in narrower cracks. For wider cracks, full-depth crack healing is required in order to achieve better mechanical performance recovery.

2. Experimental Work

2.1. Materials and Mix Proportions. The Type I ordinary Portland cement (OPC) and fine aggregates of density 2.60 g·cm^{-3}, fineness modulus 2.43, and absorption rate 1.47% were used. To prepare mortar specimens for mechanical and water permeability testing, three types of mortar mix were used: OPC, SH1, and SH2. SH1 comprised sodium carbonate (Na_2CO_3) and calcium stearate (Ca^{2+}) embedded in zeolite, which is a porous and highly adsorptive material that can accommodate ions. The proportions of Na_2CO_3, calcium stearate, and zeolite in SH1 were 1 : 0.5 : 1.5. To prepare SH1, Na_2CO_3 was dissolved in water, zeolite was added to the mix, and the mixture was dried at 40°C for 24 hours and then immediately dried at 100°C for 72 hours. Powdered healing agents passed through a 0.06 mm sieve were obtained by sieving and crushing SH1 composed of such a mix and stearate. SH2 comprised SH1 powder, calcium sulfoaluminate (CSA) as an expansion agent, and bentonite as a geomaterial, in the proportions of 3 : 2 : 1.

Table 1 lists the mix proportions by mass of the three mortar mixtures. For OPC, the mortar mixture of water : cement : sand was 0.4 : 1 : 2, and for all mixtures, the targeted slump flow was 180 ± 25 mm. In the SH1 and SH2 mixes, 1.5% and 3% of the fine aggregate content (relative to the OPC mix proportions) by mass were replaced with healing agents. To control the workability of the mortar mixture, a high range water reducing agent (HRWRA) of the polycarbonic acid type was added in the proportions of 0.5–2.5% by the mass of cement. Specimens for water permeability testing were produced using the mix proportions listed in Table 1 excluding the use of fiber. For mechanical performance evaluation, however, PVA fibers amounting to 0.5% of the total mixture's volume were used. Density, diameter, and length of the fibers were 1.3 gm/cm^3, 0.04 mm, and 6 to 12 mm, respectively. As listed in Table 1, the compressive strengths of specimens containing healing agents were lower than that of the OPC specimen; this was due to the porous nature of the self-healing agents.

2.2. Mechanical Testing. To assess the self-healing capability of mortar beams, specimens of 100 × 100 × 400 mm each having a central notch of 40 mm were prepared and cured in a water bath of temperature 20 ± 2°C for 28 days. All beam specimens were precracked at various levels of crack opening ranging from 70 to 150 μm by means of 3-point bending testing (3 PBT; Figure 1); this flexural testing was performed using a universal testing machine (UTM) with the loading capacity of 300 kN and loading rate of 0.05 mm·s^{-1}. During testing, crack mouth opening displacement (CMOD) was monitored using a clip gauge as shown in Figure 1. After achieving the targeted CMOD, the loading was stopped and released.

A high-magnification digital microscope having a lens magnification of 160x and equipped with a 1/2.9″ CMOS camera was used for the actual crack width measurement, both after precracking and before the reloading stages (Figure 2). All cracked specimens were immersed in water at 20°C for the healing periods of 28 and 56 days. Duplicated specimens were cast and tested to evaluate their mechanical performance. After the scheduled healing period, 3-point bending tests were conducted to reload the specimens and to acquire curves of load versus CMOD for comparison of the precracking and reloading responses.

Mechanical performance was evaluated in terms of two indices: the index of strength recovery (ISR) and the index of damage recovery (IDR) defined in Figure 3. These were computed as follows:

$$\mathrm{ISR} = \frac{P_{\mathrm{reloading}} - P_{\mathrm{unloading}}}{P_{\mathrm{loading}} - P_{\mathrm{unloading}}}, \quad (1)$$

$$\mathrm{IDR} = \frac{K_{\mathrm{reloading}} - K_{\mathrm{unloading}}}{K_{\mathrm{loading}} - K_{\mathrm{unloading}}}, \quad (2)$$

where P_{loading} is the peak load reached during the precracking stage, $P_{\mathrm{reloading}}$ is the peak load reached after the

Table 1: Mix proportions for the three fiber-reinforced mortar mixtures.

Mix type	Water	Cement	Fiber (vol.%)	Fine aggregate	Healing agent		f_c' (MPa)	Slump flow (mm)
					SH1	SH2		
OPC	0.40	1.00	0.5	2.00	—	—	54.6	170
SH1	0.40	1.00	0.5	1.97	0.03	—	47.3	165
SH2	0.40	1.00	0.5	1.94	—	0.06	49.6	169

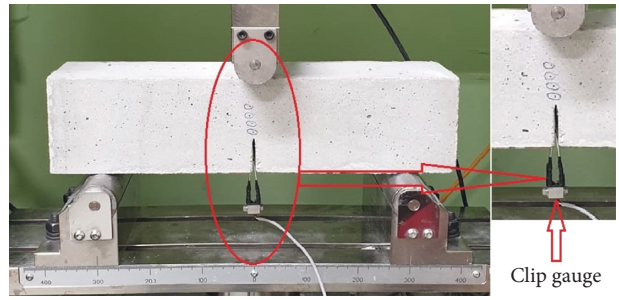

Figure 1: Three-point bending test setup.

(a) (b)

Figure 2: Microscope setup used to image cracked specimens before and after healing: (a) microscope equipped with a digital camera; (b) image capture.

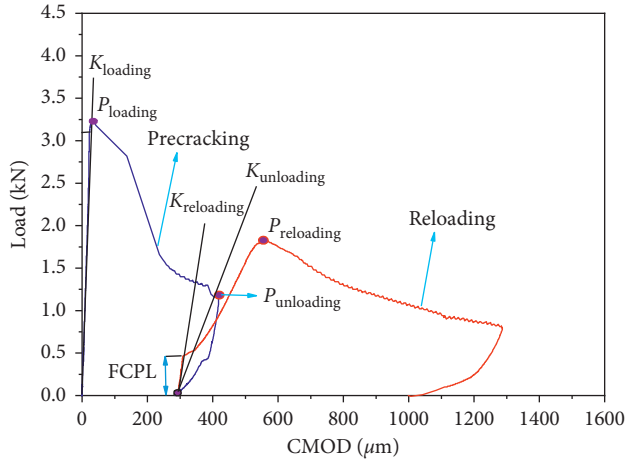

Figure 3: Load versus CMOD response during 3 PBT: (blue) precracking curve and (red) reloading curve after exposure duration. Definitions of quantities used in calculation of self-healing indices are also indicated.

reloading cycle, $P_{unloading}$ is the load at which loading was stopped during the precracking stage, $K_{loading}$ is the stiffness under half of the peak load and the corresponding CMOD during the precracking stage, $K_{reloading}$ is the initial stiffness after the reloading cycle, and $K_{unloading}$ is the stiffness at the unloading point. Figure 3 graphically depicts the definitions of these parameters. FCPL is the load when beam specimens first cracked during reloading, but the specimen could sustain additional load until the maximum point termed as $P_{reloading}$, as shown in Figure 3.

This study proposes a new technique to evaluate the mechanical performance of cracked specimens after autogenous healing, in terms of dissipation energy gain. The index of dissipation energy gain (IDEG) of a healed specimen can be determined from a stress (σ) versus CMOD curve of a notched beam specimen following a similar method suggested by RILEM [26]. The following equation was used to calculate the stress σ from the load obtained from 3 PBT:

$$\sigma = \frac{3P \cdot L}{2b(d-a)^2}, \quad (3)$$

where P is the maximum load attained by the specimen, L is the support length during 3 PBT (300 mm), b is the width of the beam (100 mm), d is the beam depth (100 mm), and a is the notch depth (40 mm).

From the stress (σ) versus CMOD diagram, the dissipation energy gain arising from self-healing can be estimated as illustrated in Figure 4. The reloading curve along the CMOD axis shifted backward until the point of $P_{\text{reloading}}$ touches the precracking curve as graphically presented in Figure 4. Then, it was assumed that Area B, which is the increment of energy dissipation due to healing, was the same as Area A. From the trend of stress (σ) versus CMOD response, the index of dissipation energy gain (IDEG) can be calculated as follows:

$$\text{IDEG} = \frac{E_{\text{D healed}}}{E_{\text{D virgin}}}, \quad (4)$$

where $E_{\text{D healed}}$ is the dissipation energy gain due to healing effect (Area A) and $E_{\text{D virgin}}$ is the total dissipation energy of the reference specimen. That is, the area under stress (σ) versus CMOD curve until stress level reaching 1.0 MPa is fixed as a benchmark as shown in Figure 4.

2.3. Water Permeability Testing. After disk specimens ($\varnothing 100 \times 50$ mm) were cured for 28 days in water at 20°C, the specimens were split using a UTM. The target crack widths were achieved by using silicon tapes of specific size, kept on both ends of semicircular specimens, and the two semicircular specimens were tied together with a steel band as shown in Figure 5(a). Crack widths were measured at 6 points on both the top and bottom sides, and the results were averaged. The constant water head permeability test method was performed to measure water flow through the cracked specimens as suggested in [27], as shown in Figure 5(b).

The targeted crack width for water permeability evaluation was 200–300 μm. Permeability testing was carried out using the healing periods of 0, 7, 14, 21, and 28 days. The self-healing index, SH_q, which is equivalent to the rate of reduction of water flow, can be obtained as follows:

$$\text{SH}_q(t) = \left(1 - \frac{q_{(t)}}{q_o}\right) \times 100\,(\%), \quad (5)$$

where $q_{(t)}$ is the water flow rate at time t and q_o is the initial water flow rate.

2.4. Microscopic Observation and Microstructural Characterization. Each specimen was microscopically observed in a high-magnification digital microscope to determine the crack length and width. After the precracking, each specimen was marked with 3 points along the crack length on the top and bottom sides, photographs were taken, and crack widths were measured at each point. All specimens were placed in a water bath for a healing period of 28 days or 56 days. After the healing process, photographs of the same marked points were retaken. The images taken before and after healing were compared to ascertain how much the cracks had sealed.

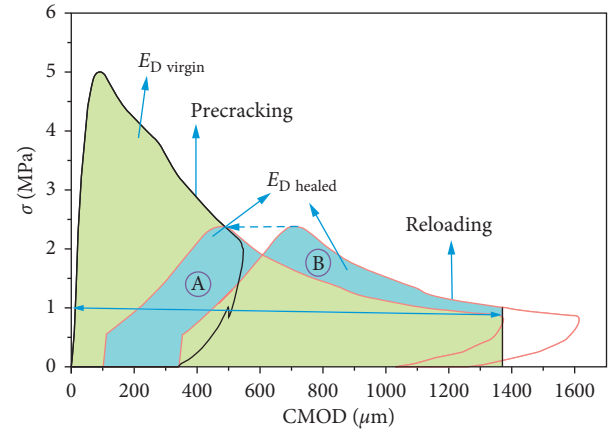

Figure 4: Schematic diagram of a curve of stress (σ) versus CMOD after crack healing, which is used for calculating the index of dissipation energy gain (IDEG).

To analyse the microstructure of the healing materials generated on the cracked surface of the cement mortar at the end of final fracture, scanning electron microscopy (SEM) and energy dispersive spectrometry (EDS) analyses were performed. The microscope used for SEM analysis was an ultrahigh-resolution field emission SEM instrument capable of imaging with magnifications ranging from 25 to 10^6. The form and structure of the self-healing products on concrete crack surfaces were confirmed using SEM, and the chemical compositions of self-healing products were analysed by means of EDS.

3. Results and Discussion

3.1. Load versus CMOD. Curves of load versus CMOD for some selected specimens were plotted after the healing periods of 28 and 56 days (Figure 6). Each curve briefly describes the trends of precracking and reloading at the end of the healing period. Within the legends of Figure 6, each first component represents the mix type: OPC, SH1, or SH2. The second represents the healing period: either 28 or 56 days. The third represents the crack width in μm. The effect of healing was evident from the curves of load versus CMOD for all mix types. Compared to OPC specimens, specimens incorporating healing agents exhibited better recovery of load-bearing capacity during the reloading stage and improved ductility.

Curves of load versus CMOD showed that the first cracking peak load (FCPL) increased when healing agents were used (Figure 6). At the healing period of 28 days, the FCPLs of SH1-28D-71 and SH2-28D-83 were 34% and 80% higher than that of OPC-28D-79, respectively, as listed in Table 2. Healing agents SH1 and SH2 contributed more to increasing FCPL for narrower cracks compared to wider cracks at the healing period of 56 days (0.48 versus 0.71); the FCPLs in these cases were, respectively, 23% and 82% higher than those of OPC. This finding is attributed to the fact that

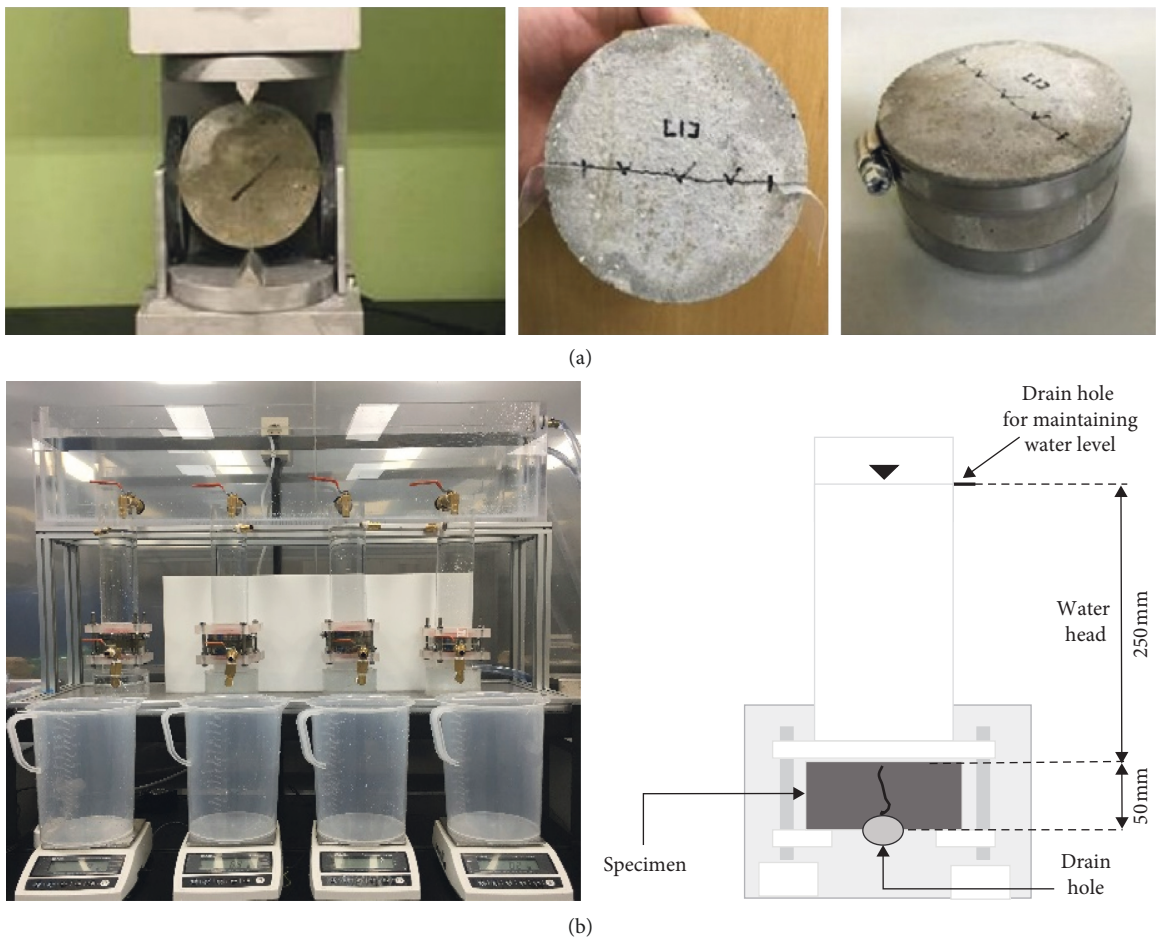

Figure 5: Preparation of cracked specimens for water permeability testing: (a) precracking; (b) water flow testing.

narrower cracks achieve full-depth healing, whereas wider crack are only partially healed; full-depth healing of wider cracks is required to achieve higher values of FCPL [28, 29].

OPC specimens showed slow and discontinuous healing because the only healing mechanism was further hydration of unhydrated cement grains. In addition, the C-S-H gel which is the main contributor to healing in OPC specimens was not sufficiently strong to carry the maximum load. For SH1 specimens, precipitation of $CaCO_3$ owing to the reaction of Ca^{2+} and $CO_3{}^{2-}$ occurred near the crack surface, which was the main contributor to crack healing at early ages. Furthermore, SH2 specimens achieved better healing compared to SH1 and OPC because they contained crystalline materials, expansive agents, and geomaterials. These constituents react more quickly with surrounding moisture, expanding in the cracked zone and sealing the crack volume by means of their extra swelling and greater expansion capacity.

3.2. Index of Strength Recovery (ISR) and Index of Damage Recovery (IDR). The mechanical parameter indices defined in Figure 3 are summarized in Tables 2 and 3, including ISR and IDR obtained by using equations (1) and (2). ISR values of all specimens are also shown in Figure 7(a) for the healing periods of 28 and 56 days. For cracks of width less than 100 μm, SH1 and SH2 specimens exhibited better strength recovery after 56 days of healing than after 28 days. Furthermore, the ISRs of SH1-56D-91 and SH2-56D-78 specimens with crack widths less than 100 μm were, respectively, 57% and 93% higher than that of OPC-56D-72. However, there was not much difference in ISRs regardless of specimen types when crack width was larger than 100 μm because bridging capacity was not enough to sustain more loads.

This finding suggests that, for specimens containing healing agents, leaching of $Ca(OH)_2$ would be possible, which generates $CaCO_3$ due to a continuous supply of moisture through the fiber interface. This extra moisture would penetrate the crack area, causing delayed hydration and speeding the healing rate. Thus, healing products are formed by means of chemical reactions involving extra water that penetrates the crack; these reactions close the crack and restore the load-bearing capacity of the material, as similarly reported in [30]. However, limited load-bearing capacity was found in the present work for crack widths greater than 140 μm because larger cracks were not completely healed throughout their depths, requiring more time for such recovery. Furthermore, considerably stronger bonding capacity of healing products was found in SH specimens

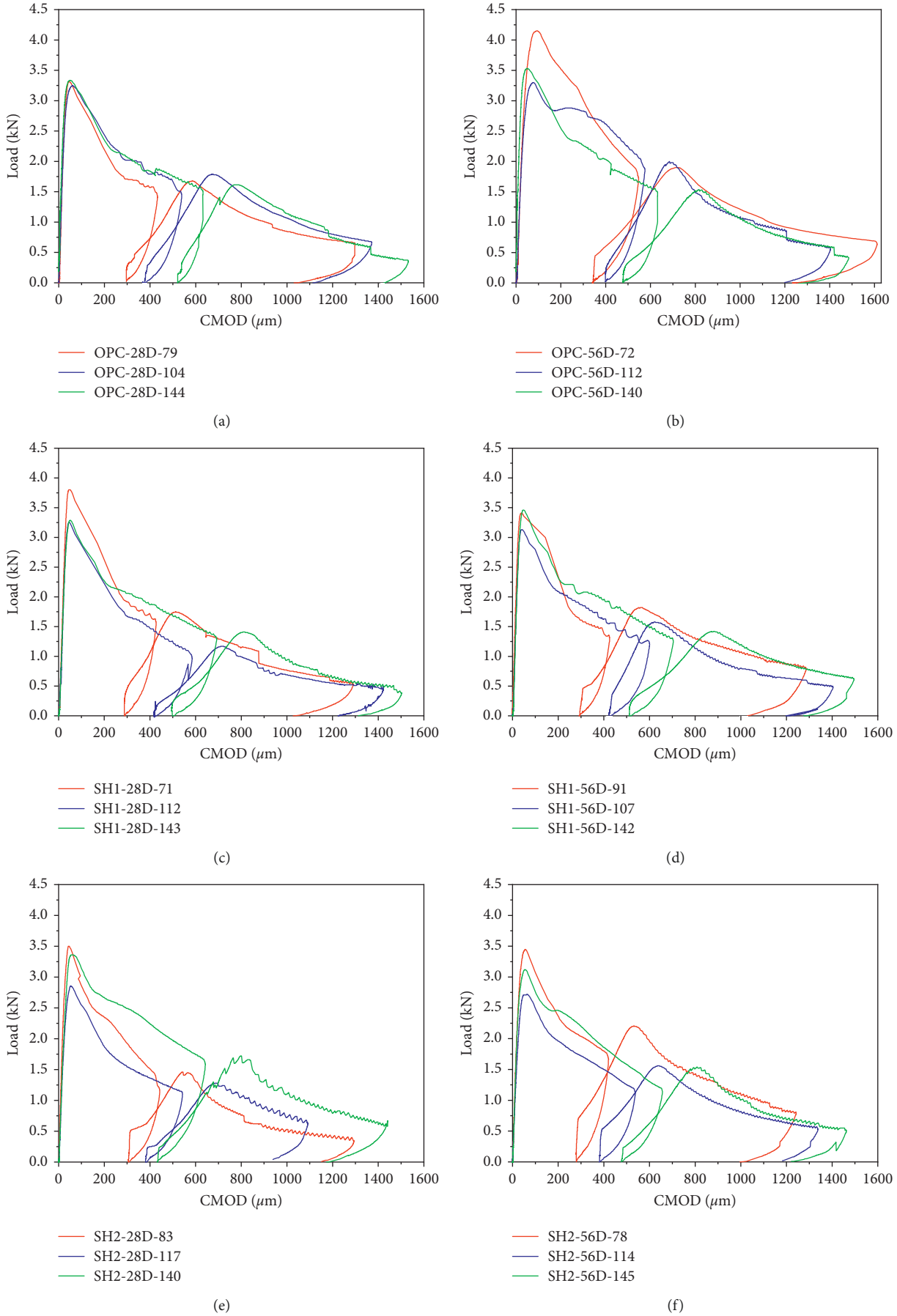

Figure 6: Load versus CMOD for specimens of all mix types, healed for durations of 28 or 56 days: (a) OPC, 28 days; (b) OPC, 56 days; (c) SH1, 28 days; (d) SH1, 56 days; (e) SH2, 28 days; (f) SH2, 56 days.

Table 2: Mechanical recovery indices for three mixes at 28 days of healing.

Type	W (μm)	FCPL (kN)	$P_{loading}$ (kN)	$P_{unloading}$ (kN)	$P_{reloading}$ (kN)	$K_{loading}$ (MPa)	$K_{unloading}$ (MPa)	$K_{reloading}$ (MPa)	ISR	IDR
OPC-28D	75	0.31	3.07	1.21	1.44	109	9.1	25	0.12	0.16
	79	0.26	3.31	1.50	1.68	110	12.0	29	0.10	0.17
	104	0.28	3.25	1.55	1.70	108	7.6	23	0.09	0.15
	109	0.23	3.46	1.68	1.85	114	8.4	22	0.10	0.13
	144	0.19	3.18	1.49	1.61	107	7.8	19	0.07	0.11
	146	0.38	2.83	1.52	1.65	107	8.4	20	0.10	0.12
SH1-28D	71	0.35	3.83	1.50	1.80	95	11.0	30	0.13	0.23
	74	0.39	3.52	1.55	1.81	100	15.0	33	0.13	0.21
	107	0.27	3.8	1.36	1.65	104	8.0	25	0.12	0.18
	112	0.19	3.25	1.09	1.33	80	6.1	19	0.11	0.17
	140	0.22	3.25	1.29	1.42	87	7.2	20	0.07	0.16
	143	0.20	3.29	1.32	1.47	110	6.8	21	0.08	0.14
SH2-28D	81	0.49	4.23	1.77	2.14	124	9.3	48	0.15	0.34
	83	0.47	3.50	1.18	1.49	120	8.5	50	0.13	0.37
	113	0.29	3.0	1.52	1.72	71	9.7	25	0.14	0.25
	117	0.26	2.86	1.13	1.31	88	6.9	27	0.10	0.25
	134	0.22	3.36	1.59	1.77	89	7.5	22	0.10	0.18
	140	0.24	2.96	1.57	1.71	91	9.0	20	0.10	0.13

Table 3: Mechanical recovery indices for three mixes at 56 days of healing.

Type	W (μm)	FCPL (kN)	$P_{loading}$ (kN)	$P_{unloading}$ (kN)	$P_{reloading}$ (kN)	$K_{loading}$ (MPa)	$K_{unloading}$ (MPa)	$K_{reloading}$ (MPa)	ISR	IDR
OPC-56D	72	0.39	4.00	1.54	1.88	99	8.2	29	0.14	0.23
	73	0.36	4.15	1.59	1.93	98	8.5	31	0.13	0.25
	110	0.24	3.28	1.85	1.98	88	10.0	22	0.09	0.15
	112	0.26	3.30	1.86	2.01	75	15.0	22	0.10	0.12
	140	0.23	3.46	1.37	1.57	150	8.9	25	0.10	0.11
SH1-56D	82	0.46	3.23	1.10	1.51	117	8.7	42	0.19	0.31
	91	0.48	3.41	1.36	1.81	136	13.0	54	0.22	0.33
	107	0.33	3.13	1.21	1.56	104	6.9	29	0.18	0.23
	110	0.35	3.11	1.72	1.84	84	9.5	25	0.09	0.21
	142	0.21	3.46	1.28	1.53	98	6.8	23	0.11	0.18
	147	0.18	2.73	1.20	1.36	91	6.2	18	0.10	0.14
SH2-56D	78	0.71	3.45	1.74	2.21	113	9.0	75	0.27	0.63
	85	0.69	3.50	1.71	2.15	100	14	68	0.25	0.63
	111	0.50	2.72	1.18	1.48	91	7.2	35	0.19	0.33
	114	0.57	3.03	1.38	1.68	86	8.8	43	0.18	0.44
	143	0.30	3.65	1.29	1.69	104	5.0	27	0.17	0.22
	145	0.26	3.20	1.22	1.54	110	6.8	29	0.16	0.22

relative to OPC, which can be directly attributed to increased ISR.

Recovery of mechanical performance in terms of IDR is plotted in Figure 7(b). A substantial increase in IDR was observed in SH2-56D-78; its IDR was about 91% and 173% higher than that of SH1-56D-91 and OPC-56D-72, respectively. The IDR trends presented in Figure 7(b) showed a steeper slope than ISR at a similar crack width, demonstrating that adding healing agents increased not only the load carrying capacity but also stiffness of the cracked specimen; this ultimately results in long-term ductility and sustainability of structures.

Mechanical performance recovery in terms of IDR was more prominent than that of ISR for narrower crack widths, indicating that healing agents filled nearly the entirety of the crack, thereby making the mortar surface denser and stronger. This was possible because healing materials generate $CaCO_3$ products upon reaction with surrounding moisture supplied by fiber through fiber interface as described elsewhere [17, 31, 32].

3.3. Index of Dissipation Energy Gain (IDEG). Energy dissipation occurred within the fracture process zone, which is the region in front of the crack tip where stress decreases as the crack opens. Table 4 summarizes the values of E_D and IDEG for OPC, SH1, and SH2 specimens, calculated after the healing periods of 28 and 56 days by using equation (4). Figure 7(c) shows the graph of the values of IDEG for all specimens. The test results demonstrated that greater values of IDEG resulted from the larger $E_{D\,healed}$, namely, the greater energy dissipated during the healing process. Even though higher IDEG was achieved especially in SH specimens with

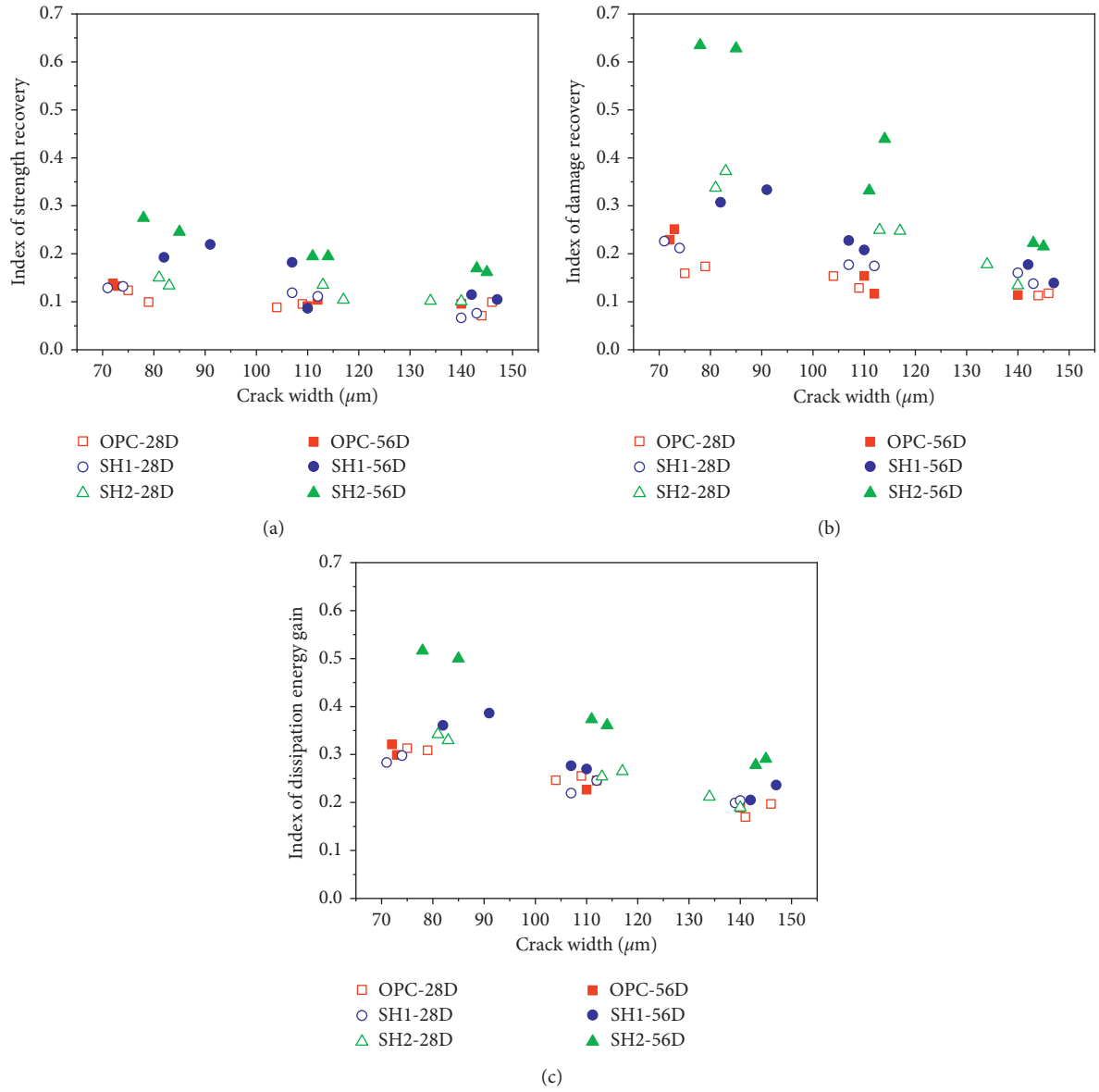

Figure 7: Indices of mechanical performance versus crack width: (a) index of strength recovery (ISR); (b) index of damage recovery (IDR); (c) index of dissipation energy gain (IDEG).

crack widths less than 100 μm, better dissipated energy gain was achieved even for OPC specimens regardless of the crack width as compared to the recovery of strength and damage, as evident from Figure 7(c).

Healing not only contributes to crack closure but also enhances load carrying capacity during the reloading stage. More energy was restored by crack healing and found to be significant in SH2 specimens. Moreover, the increase of dissipated energy due to healing is totally dependent on the interconnection between crack flanks as well as full-depth crack healing [28, 29].

Based on the findings of the present study, we suggest that the proposed technique based on the IDEG is appropriate to evaluate the effects of healing on the resistance to external loadings, which is related to energy dissipations such as from earthquakes, impacts, and explosions.

3.4. Water Permeability. Watertightness and durability in concrete structures would be assessed in terms of water permeability properties, so the water flow rate was quantified to investigate time-dependent permeability characteristics of cracked mortar specimens. As shown in Figure 8, which shows water flow rates for OPC, SH1, and SH2 specimens at the healing periods of 0, 7, 14, 21, and 28 days, the water flow rate decreased more when healing agents were used. Based on the test results in Figure 8 showing water flow rate versus healing duration, the values of the self-healing index obtained using equation (5) are listed in Table 5. Because healing products restricted the water flow during testing, SH1 and SH2 specimens showed greater reductions in water flow rate compared to OPC specimens. That is, quick formation of crystalline products near the cracked zone ensured crack sealing, which in turn

Table 4: Calculated dissipation energy gain under stress (σ) vs. CMOD curve, index of dissipation energy gain (IDEG) for different mix types.

Mix type	Crack width (μm)	E_D (N/mm)		IDEG
		$E_{D\,virgin}$	$E_{D\,healed}$	
OPC-28D	75	1.31	0.41	0.31
	79	1.49	0.46	0.31
	104	2.11	0.52	0.25
	109	2.27	0.58	0.26
	141	1.12	0.19	0.17
	146	1.27	0.25	0.20
OPC-56D	72	1.09	0.35	0.32
	73	0.97	0.29	0.30
	110	0.75	0.17	0.23
	112	0.57	0.14	0.25
	140	0.90	0.17	0.19
SH1-28D	71	1.80	0.51	0.28
	74	1.78	0.53	0.30
	107	2.14	0.47	0.22
	112	2.24	0.55	0.25
	139	1.96	0.39	0.20
	140	2.06	0.42	0.20
SH1-56D	82	1.33	0.48	0.36
	91	1.01	0.39	0.39
	107	2.17	0.60	0.28
	110	2.04	0.55	0.27
	142	0.78	0.16	0.21
	147	1.65	0.39	0.24
SH2-28D	81	1.90	0.65	0.34
	83	1.76	0.58	0.33
	113	1.93	0.49	0.25
	117	1.85	0.49	0.26
	134	2.36	0.50	0.21
	140	2.06	0.39	0.19
SH2-56D	78	1.53	0.79	0.52
	85	1.70	0.85	0.50
	111	1.42	0.53	0.37
	114	1.33	0.48	0.36
	143	1.87	0.52	0.28
	145	1.72	0.50	0.29

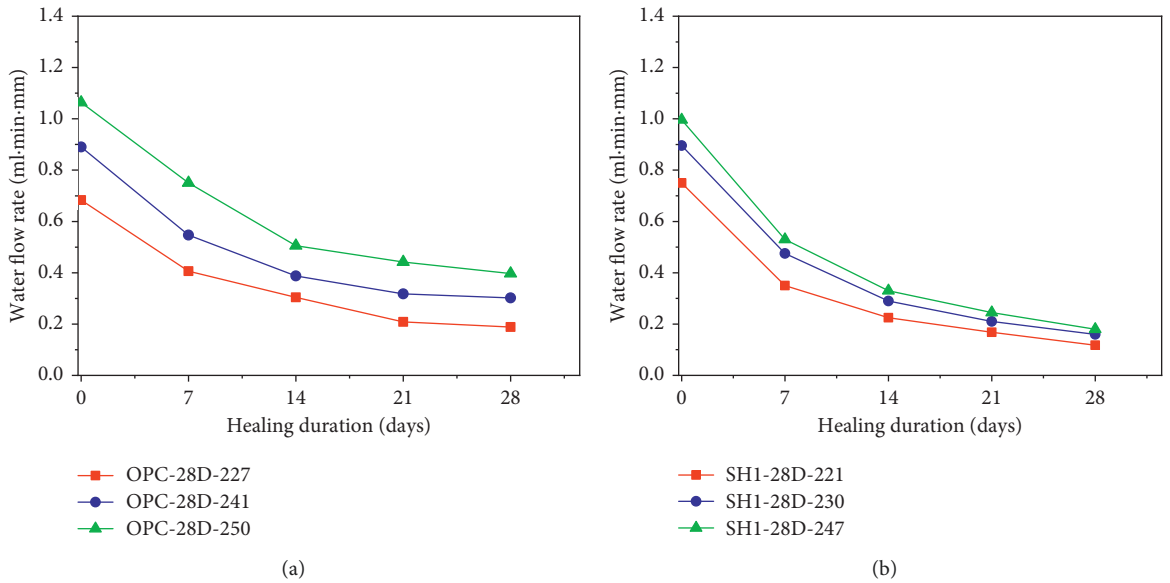

Figure 8: Continued.

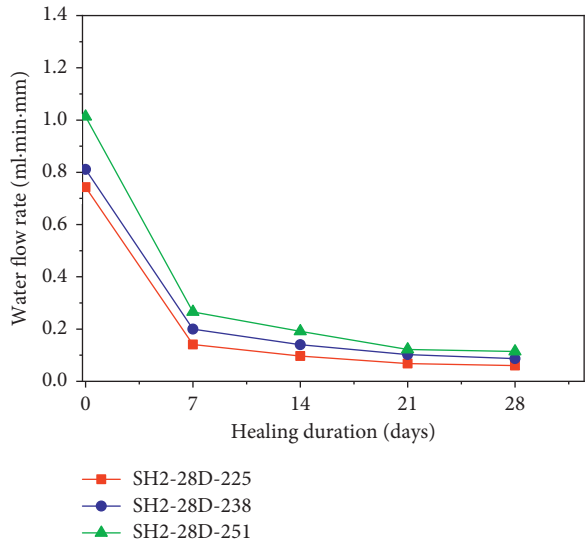

(c)

Figure 8: Water flow rate versus healing duration for three mixes at the healing periods of 0, 7, 14, 21, and 28 days: (a) OPC; (b) SH1; (c) SH2.

Table 5: Water flow rate and self-healing indices of the three mixes.

Mix type	Crack width (μm)	Water flow ($ml \cdot mm^{-1} \cdot min^{-1}$)		Self-healing index SH_w (%)
		Q_0	Q_{28}	
OPC-28D-227	227	0.68	0.19	72.4
OPC-28D-241	241	0.89	0.30	66.0
OPC-28D-250	250	1.06	0.40	63.0
SH1-28D-221	221	0.75	0.12	84.3
SH1-28D-230	230	0.90	0.16	82.2
SH1-28D-247	247	1.00	0.18	81.9
SH2-28D-225	225	0.74	0.06	91.9
SH2-28D-238	238	0.81	0.09	89.3
SH2-28D-251	251	1.01	0.11	88.7

heightened the water flow decrease rate to more than that of OPC. Meanwhile, the OPC specimens showed less C-S-H gel content due to delayed hydration and insufficient generation of crystalline products near the crack. In addition, there was more gap between interconnecting healed particles. Thus, the water flow rate was not much influenced by such crack sealing.

Moreover, for SH2, crack sealing restricted the water flow rate by up to 90%, while the mechanical performance enhancements in terms of ISR, IDR, and IDEG at 28 days of healing were 14%, 37%, and 35%, respectively, for crack widths less than 100 μm. That is, the water flow reduction rate was found to be greater than the mechanical performance enhancement. This is due to the fact that calcium carbonate precipitation, extra expansion, and swelling of geomaterials would seal the crack volume and reduce air voids of healed products, which can restrict the water flow by reducing the velocity of flowing water [23, 33].

3.5. Microscopic Observation and SEM Analysis. Digital microscope images of cracked areas showed remarkable crack sealing in cracked specimens incorporating self-healing agents (Figure 9). This is because healing agents generated more healing products near the crack surface upon reaction with surrounding moisture, and these healing products then accumulated at the crack surface as white residue, as shown in Figure 9. The crack surface closing was almost 80% at the healing period of 56 days in SH1 and SH2 specimens, confirming the effectiveness of healing agents in crack sealing at the early stages of healing.

The self-healing products of OPC, SH1, and SH2 were identified using SEM imaging and EDS analysis. Figure 10 shows SEM images of the cracked area at the healing period of 56 days. The crack surfaces of OPC had not yet been filled, but calcium carbonate had formed to cover the surface, confirming the elution of calcium carbonate. In the crack surfaces of SH1 and SH2, substances that would become self-healing products were identified. SH1 produced self-healing

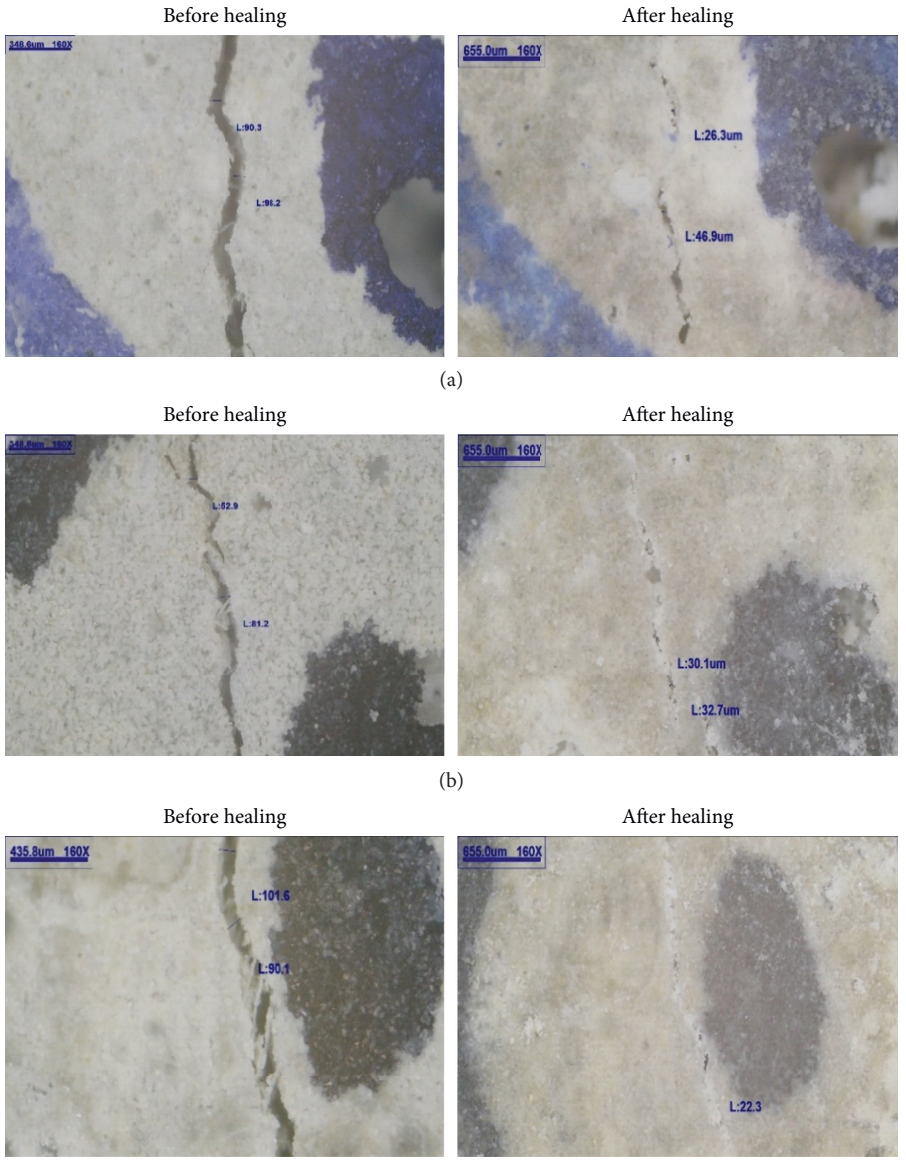

Figure 9: Microscopic observation of specimens before and after the healing period of 56 days in water immersion conditions: (a) OPC; (b) SH1; (c) SH2.

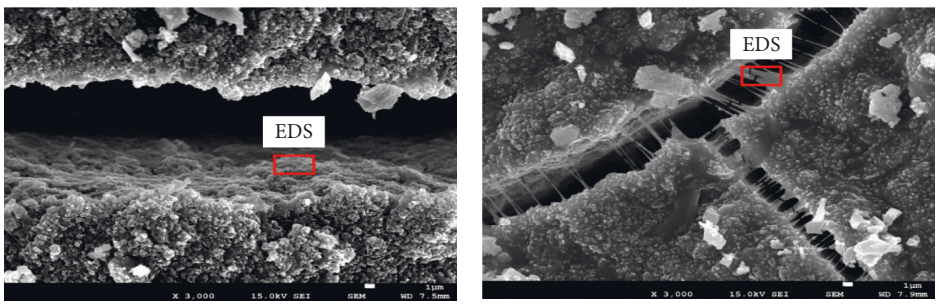

Figure 10: Continued.

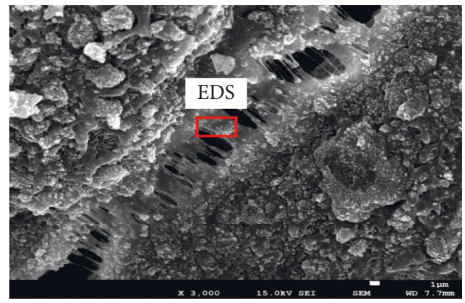

(c)

Figure 10: SEM image of crack surfaces after 56 days of healing (×3,000 magnification): (a) OPC; (b) SH1; (c) SH2.

products having thin bridges, whereas SH2 produced large quantities of the self-healing products.

Table 6 shows the EDS analysis results of crack surfaces of OPC, SH1, and SH2. A SEM image showed $CaCO_3$ on the crack surface of the OPC; the sum of the present constituents of O, Ca, and C was 96.4% in OPC. Furthermore, the Ca and Si content increased, and O content decreased in SH1 and SH2. In addition, Na was detected in the self-healing products of SH1 and SH2, composed of zeolite impregnated with Na_2CO_3, and Al was detected only in SH2, which incorporated a CSA expansive agent. This confirmed the observation of both $CaCO_3$ and ettringite on the crack surface of SH2, whereas most of the compounds found on the crack surfaces in OPC and SH1 were $CaCO_3$. Accordingly, self-healing materials could generate healing products on the crack surfaces of the specimen, resulting in crack sealing.

Table 6: EDS analysis results of mortar crack surfaces.

Mix type	C	O	K	Si	Na	Al	Ca	Other	Total
OPC	21.8	50.2	0.4	2.7	—	—	24.4	0.5	100
SH1	20.3	28.9	0.9	19.2	2.6	—	28.1	0.0	100
SH2	14.6	30.2	0.6	11.7	3.7	4.2	34.9	0.1	100

4. Conclusions

The following conclusions are drawn from the present experimental study on stimulated autogenous healing in cracked fiber-reinforced mortars incorporating healing agents:

(1) Healing agents such as crystalline materials, expansive agents, and geomaterials increase the mechanical performance recovery of cracked fiber-reinforced mortar specimens by means of rapid recrystallization and calcium carbonate precipitation. Cracks of width less than 100 μm were effectively healed with respect to their ISR and IDR.

(2) Improved energy dissipation capacity was observed when compared to strength and damage recovery at the same crack widths. This suggests that crack healing due to the use of healing material contributes to increased energy dissipation and controls the crack propagation effect, ultimately resulting in greater resistance by the structure against sudden damage and structural collapse. Thus, finding IDEG with the addition of healing agents proved to be more appropriate in evaluating the mechanical performance of concrete structures. Also, SEM and EDS analysis confirmed the presence of healing products such as $CaCO_3$ on the crack surfaces.

(3) Since healing agents produce more crystalline products near the crack surfaces, water tightness was found to be more than 90% in the SH specimen. In addition, the self-healing index of water flow rate for specimens incorporating healing agents was considerably higher than that for OPC specimens. This confirms healing agents could play a major role in improving the watertightness of concrete.

(4) Healing agents contributed to increasing watertightness, resulting in more enhanced surface crack sealing capacity when compared to their mechanical performance enhancement in both smaller and wider cracks. This finding is attributed to the fact that mechanical performance recovery is based on full-depth crack healing as well as resistance between interconnecting healed particles, which can be improved by further increasing the healing duration. Therefore, it is of utmost importance to evaluate the water permeability as well as the mechanical performance of self-healing materials in order to ensure the sustainability of concrete structures.

Data Availability

The (Excel type) data used to support the findings of this study are available from the corresponding author upon request.

Conflicts of Interest

The authors declare that there are no conflicts of interest regarding the publication of this paper.

Acknowledgments

This research was supported by a grant (19SCIP-B103706-05) from Construction Technology Research Program funded by the Ministry of Land, Infrastructure and Transport of the Korean government. This research received funding from the Korean government.

References

[1] K. Van Tittelboom and N. De Belie, "Self-healing in cementitious materials—A review," *Materials*, vol. 6, no. 6, pp. 2182–2217, 2013.

[2] L. Ferrara, T. Van Mullem, M. C. Alonso et al., "Experimental characterization of the self-healing capacity of cement based materials and its effects on the material performance: a state of the art report by COST Action SARCOS WG2," *Construction and Building Materials*, vol. 167, pp. 115–142, 2018.

[3] F. U. R. Abro, A. S. Buller, K.-M. Lee, and S. Y. Jang, "Using the steady-state chloride migration test to evaluate the self-healing capacity of cracked mortars containing crystalline, expansive, and swelling admixtures," *Materials*, vol. 12, no. 11, p. 1865, 2019.

[4] H. Huang, G. Ye, C. Qian, and E. Schlangen, "Self-healing in cementitious materials: materials, methods and service conditions," *Materials & Design*, vol. 92, pp. 499–511, 2016.

[5] K. B. Shim, T. Kishi, C.-S. Choi, and T.-H. Ahn, "Cementitiuous materials for crack self-healing concrete," *Journal of Ceramic Processing Research*, vol. 16, pp. 1–13, 2015.

[6] K. Van Tittelboom, N. De Belie, W. De Muynck, and W. Verstraete, "Use of bacteria to repair cracks in concrete," *Cement and Concrete Research*, vol. 40, no. 1, pp. 157–166, 2010.

[7] H. M. Jonkers, A. Thijssen, G. Muyzer, O. Copuroglu, and E. Schlangen, "Application of bacteria as self-healing agent for the development of sustainable concrete," *Ecological Engineering*, vol. 36, no. 2, pp. 230–235, 2010.

[8] C. Kang, J. Huh, Q. H. Tran, and K. Kwak, "Evaluation of self-healing performance of PE and PVA concrete using flexural test," *Advances in Materials Science and Engineering*, vol. 2018, Article ID 6386280, 10 pages, 2018.

[9] F. Dell'Isola, I. Giorgio, and U. Andreaus, "Elastic pantographic 2D lattices: a numerical analysis on the static response and wave propagation," *Proceedings of the Estonian Academy of Sciences*, vol. 64, no. 3, pp. 219–225, 2015.

[10] F. Dell'Isola, P. Seppecher, J. J. Alibert et al., "Pantographic metamaterials: an example of mathematically driven design and of its technological challenges," *Continuum Mechanics and Thermodynamics*, vol. 31, no. 4, pp. 851–884, 2019.

[11] C. Boutin, F. Dell'Isola, I. Giorgio, and L. Placidi, "Linear pantographic sheets: asymptotic micro-macro models identification," *Mathematics and Mechanics of Complex Systems*, vol. 5, no. 2, pp. 127–162, 2017.

[12] H. Deng and G. Liao, "Assessment of influence of self-healing behavior on water permeability and mechanical performance of ECC incorporating superabsorbent polymer (SAP) particles," *Construction and Building Materials*, vol. 170, pp. 455–465, 2018.

[13] T.-H. Ahn and T. Kishi, "The effect of geo-materials on the autogenous healing behavior of cracked concrete," in *Concrete Repair, Rehabilitation and Retrofitting II*, CRC Press, Boca Raton, FL, USA, 2008.

[14] L. Placidi, "A variational approach for a nonlinear 1-dimensional second gradient continuum damage model," *Continuum Mechanics and Thermodynamics*, vol. 27, no. 4-5, pp. 623–638, 2015.

[15] L. Placidi, E. Barchiesi, and A. Misra, "A strain gradient variational approach to damage: a comparison with damage gradient models and numerical results," *Mathematics and Mechanics of Complex Systems*, vol. 6, no. 2, pp. 77–100, 2018.

[16] A. Rinaldi and L. Placidi, "A microscale second gradient approximation of the damage parameter of quasi-brittle heterogeneous lattices," *ZAMM—Journal of Applied Mathematics and Mechanics/Zeitschrift für Angewandte Mathematik und Mechanik*, vol. 94, no. 10, pp. 862–877, 2014.

[17] L. Ferrara, V. Krelani, and M. Carsana, "A "fracture testing" based approach to assess crack healing of concrete with and without crystalline admixtures," *Construction and Building Materials*, vol. 68, pp. 535–551, 2014.

[18] T. Nishiwaki, S. Kwon, D. Homma, M. Yamada, and H. Mihashi, "Self-healing capability of fiber-reinforced cementitious composites for recovery of watertightness and mechanical properties," *Materials*, vol. 7, no. 3, pp. 2141–2154, 2014.

[19] H. Choi, M. Inoue, S. Kwon, H. Choi, and M. Lim, "Effective crack control of concrete by self-healing of cementitious composites using synthetic fiber," *Materials*, vol. 9, no. 4, 2016.

[20] E. Herbert and V. Li, "Self-healing of microcracks in engineered cementitious composites (ECC) under a natural environment," *Materials*, vol. 6, no. 7, pp. 2831–2845, 2013.

[21] K. Van Tittelboom, E. Gruyaert, H. Rahier, and N. De Belie, "Influence of mix composition on the extent of autogenous crack healing by continued hydration or calcium carbonate formation," *Construction and Building Materials*, vol. 37, pp. 349–359, 2012.

[22] T.-H. Ahn and T. Kishi, "Crack self-healing behavior of cementitious composites incorporating various mineral admixtures," *Journal of Advanced Concrete Technology*, vol. 8, no. 2, pp. 171–186, 2010.

[23] T. Qureshi, A. Kanellopoulos, and A. Al-Tabbaa, "Autogenous self-healing of cement with expansive minerals-I: impact in early age crack healing," *Construction and Building Materials*, vol. 192, pp. 768–784, 2018.

[24] Y. S. Lee and J. S. Ryou, "Crack healing performance of PVA-coated granules made of cement, CSA, and Na2CO3 in the cement matrix," *Materials*, vol. 9, no. 7, p. 555, 2016.

[25] K. Sisomphon, O. Copuroglu, and E. A. B. Koenders, "Self-healing of surface cracks in mortars with expansive additive and crystalline additive," *Cement and Concrete Composites*, vol. 34, no. 4, pp. 566–574, 2012.

[26] RILEM, "Draft recommendation: determination of the fracture energy of mortar and concrete by means of three-point bend tests on notched beams," *Materials and Structures*, vol. 18, no. 6, pp. 285–290, 1985.

[27] K. J. Shin, W. Bae, S.-W. Choi, M. W. Son, and K. M. Lee, "Parameters influencing water permeability coefficient of cracked concrete specimens," *Construction and Building Materials*, vol. 151, pp. 907–915, 2017.

[28] E. Ahn, H. Kim, S. H. Sim, S. W. Shin, and M. Shin, "Principles and applications of ultrasonic-based nondestructive methods for self-healing in cementitious materials," *Materials*, vol. 10, no. 3, p. 278, 2017.

[29] T. Danner, U. Hjorth Jakobsen, and M. R. Geiker, "Mineralogical sequence of self-healing products in cracked marine concrete," *Minerals*, vol. 9, no. 5, p. 284, 2019.

[30] R. P. Borg, E. Cuenca, E. M. Gastaldo Brac, and L. Ferrara, "Crack sealing capacity in chloride-rich environments of mortars containing different cement substitutes and crystalline admixtures," *Journal of Sustainable Cement-Based Materials*, vol. 7, no. 3, pp. 141–159, 2018.

[31] K. Hannawi, H. Bian, W. Prince-Agbodjan, and B. Raghavan, "Effect of different types of fibers on the microstructure and the mechanical behavior of ultra-high performance fiber-reinforced concretes," *Composites Part B: Engineering*, vol. 86, pp. 214–220, 2016.

[32] D. Snoeck and N. De Belie, "Mechanical and self-healing properties of cementitious composites reinforced with flax and cottonised flax, and compared with polyvinyl alcohol fibres," *Biosystems Engineering*, vol. 111, no. 4, pp. 325–335, 2012.

[33] M. Roig-Flores, F. Pirritano, P. Serna, and L. Ferrara, "Effect of crystalline admixtures on the self-healing capability of early-age concrete studied by means of permeability and crack closing tests," *Construction and Building Materials*, vol. 114, pp. 447–457, 2016.